

1 **A CMIP6 ensemble for downscaled monthly climate normals over**
2 **North America**

3 Colin R. Mahony^{1*}, Tongli Wang², Andreas Hamann³, and Alex J. Cannon⁴

4

5 1. British Columbia Ministry of Forests, Lands, Natural Resource Operations and Rural
6 Development, Victoria, BC, Canada.

7 2. Centre for Forest Conservation Genetics, Department of Forest and Conservation
8 Sciences, Faculty of Forestry, University of British Columbia, Canada

9 3. Department of Renewable Resources, Faculty of Agricultural, Life, and Environmental
10 Sciences, University of Alberta, Canada

11 4. Climate Research Division, Environment and Climate Change Canada, Victoria, British
12 Columbia, Canada

13 *Correspondence to colin.mahony@gov.bc.ca; twitter @ColinRMahony

14

15 **Abstract**

16 Many studies of climate change impacts and adaptation use climate model projections
17 downscaled at very high spatial resolution (~1km) but very low temporal resolution (20- to 30-
18 year normals). These applications have model selection priorities that are distinct from analyses
19 at high temporal resolution. Here, we select a 13-model CMIP6 ensemble designed for robust
20 change-factor downscaling of monthly climate normals and describe its attributes in North
21 America. The ensemble is representative of the distribution of equilibrium climate sensitivity and
22 grid resolution in the CMIP6 generation. We provide rationale for an 8-member subset of the
23 ensemble based on screening criteria and sequence these 8 models for selection of smaller
24 ensembles for regional analysis. Although we have focused our documentation on North
25 America, the 13-model ensemble is selected using global criteria and applicable to downscaling
26 climate normals in other continents.

27

28 **Keywords:** Climate change, downscaling, model selection, CMIP6, North America.

29

30 1 Introduction

31 The most recent iteration of the Coupled Model Intercomparison Project (CMIP6; Eyring
32 et al. 2016) is a once-in-a-decade update to projections of climate change. CMIP6 provides a
33 larger number of simulations from a new generation of global climate models, at higher spatial
34 resolution, and using an improved set of emissions scenarios relative to its predecessor, CMIP5
35 (Taylor et al. 2012). These new climate simulations contribute to and are put into broader context
36 by the Sixth Assessment Report from Working Group I of the Intergovernmental Panel on
37 Climate Change (Lee et al. 2021). CMIP6 simulations are rapidly being incorporated into
38 downscaled climate data products for use in regional climate change impacts and adaptation
39 initiatives. These initiatives can benefit from careful selection of climate model projections that
40 are suited to broad classes of end uses, and their wide application requires transparency on the
41 attributes of these ensembles.

42 Many climate change impact analyses, particularly in ecology, use projections of climate
43 change that are downscaled to very high resolution (~1km) but very low temporal resolution (20-
44 to 30-year climate normals). The prevalence of this type of analysis is evident from the
45 widespread use of WorldClim (Hijmans et al. 2005, Fick and Hijmans 2017; 23340 citations) and
46 ClimateNA (Wang et al. 2012, 2016, Hamann et al. 2013; 1678 citations). The low temporal
47 resolution of these applications simplifies downscaling; both WorldClim and ClimateNA use
48 change-factor downscaling, also called the climate imprint method (Hunter and Meentemeyer
49 2005) and simple mean bias correction (Maraun 2016). This method adds low-spatial-resolution
50 anomalies from the climate model to a high-resolution gridded climate map (Tabor and Williams
51 2010). The best practices for change-factor downscaling to high-spatial and low-temporal
52 resolution are different than those for the more sophisticated statistical downscaling techniques
53 necessary for high temporal resolution downscaling (Wilby et al. 2004), leading to distinct model
54 selection priorities.

55 One consideration in model selection for change-factor downscaling is the number of
56 simulation runs for each candidate model. The change-factor method is sensitive to the influence
57 of natural variability in the historical reference period against which anomalies are calculated
58 and bias correction is applied. Similarly, natural variability during the projected future periods
59 adds “noise” to the climate change “signal” (Hui et al. 2020), the latter being of primary interest
60 to analyses of projected climate normals. Performing change-factor downscaling with multiple
61 simulations runs of each model reduces the confounding influence of natural variability in bias
62 correction and improves the signal-to-noise ratio (Milinski et al. 2019). Consequently, models
63 with multiple simulations for each historical and future scenario are preferable in this context.

64 Another consideration is the model bias. All climate models exhibit biases--systematic
65 differences between observations and simulations—at the regional scale. Removal of these
66 biases is a basic step in downscaling (Maraun 2016). Change-factor downscaling performs
67 univariate bias correction and therefore may not conserve the physical (e.g., thermodynamic)
68 interdependence between variables such as temperature and precipitation (Cannon 2018). The
69 associated potential for univariate downscaling to produce physically implausible climatic
70 conditions presumably increases with the size of the biases in the simulation. For this reason,
71 models with small biases are preferable to models with large biases, all else being equal.

72 Finally, the spatial resolution of climate models is of interest to high spatial resolution
73 downscaling. Some models contributing to the CMIP6 ScenarioMIP (O'Neill et al. 2016)
74 experiment (the candidate pool for ensemble selection in this study) have horizontal grid
75 resolutions of 70-100km. These medium-resolution models are able to resolve macrotopography,
76 e.g., to differentiate the major mountain ranges of the Western Cordillera. The opportunity to
77 better represent the influences of water bodies and topography on climate change trends, such as
78 elevation-dependent warming (Salathé et al. 2008, Palazzi et al. 2019), is appealing for climate
79 change impact analyses. Conversely, models with very low spatial resolution (>300km) can
80 conflate the climate change signals of distinct regions, particularly at land/ocean transitions
81 (Lanzante et al. 2018). Very low resolution therefore is a consideration for exclusion from
82 ensembles designed for high-resolution change-factor downscaling.

83 Collectively, the three considerations described above suggest an ensemble that prioritizes
84 number of simulations per model rather than number of models, low-to-moderate bias, and
85 moderate-to-high spatial resolution.

86 Once a general-purpose ensemble is selected, it is useful to structure the ensemble for
87 further user-specific model selection. Many applications of projected climate normals are
88 computationally intensive analyses at regional scales. In these cases, it can be desirable to use a
89 small number (3-8) of models that represent the approximate range of a more comprehensive
90 ensemble. Cannon (2015) describes a method for structuring an ensemble into an order of subset
91 selection that optimally represents the ensemble spread. Alternatively, analysts may wish to
92 select a custom subset of the ensemble. Documentation of the attributes of the ensemble
93 members can help analysts to identify subsets that are best suited to specific applications.

94 The purpose of this study is to select and describe an ensemble of CMIP6 model
95 projections of 21st century climate change over North America. The focus of model selection is
96 on facilitating robust downscaling of projected climate normals at very high spatial resolution.
97 We characterize the attributes, biases, and climate change trends of the ensemble and highlight
98 features of interest in individual climate models. Finally, we provide ordered subsets of the
99 ensemble for regional analyses and considerations for selection of custom subsets. This
100 information is complemented by an interactive web application to explore the ensemble in more
101 detail (<https://bcgov-env.shinyapps.io/cmip6-NA/>).

102 **2 Methods**

103 **2.1 Criteria for model selection**

104 We assessed all models in the ESGF holdings for the CMIP6 ScenarioMIP as of December
105 15, 2020. We selected models using six objective criteria, listed below with rationale:

- 106 • **Criterion 1: T_{\min} and T_{\max} available.** Mean daily minimum temperature (T_{\min}) and
107 mean daily maximum temperature (T_{\max}) are the directly measured elements of the long-
108 term temperature record, and are the fundamental temperature elements in many climate
109 change impact analyses.

- 110 • **Criterion 2: Minimum of 3 historical runs available.** This criterion ensures robust
111 downscaling by reducing the confounding influence of natural variability in bias
112 correction.
- 113 • **Criterion 3. Complete scenarios.** Models need to have at least one simulation for three
114 of the four major SSP marker scenarios (SSP1-2.6, SSP2-4.5, SSP3-7.0, and SSP5-8.5).
- 115 • **Criterion 4. One model per institution.** This criterion is a widely applied best practice
116 in ensemble selection (Leduc et al. 2016) as one measure to increase independence
117 among ensemble members. For the purposes of this criterion, different physics or forcing
118 schemes of the same model were considered different models.
- 119 • **Criterion 5. No closely related models.** Models that share components were excluded,
120 following Figure 5 of Brunner et al. (2019).
- 121 • **Criterion 6. No large biases.** Bias is the degree to which a model simulation differs
122 from the observed climate over a reference period (1961-1990 in this case). Models with
123 large biases relative to the rest of the ensemble in one or more variables were excluded.

124 2.2 *Ensemble subset criteria*

125 Users of the ensemble may wish or need to use a lesser number of models in their analyses.
126 To support the selection of subsets, we structure the ensemble by defining an order of exclusion
127 of models. Models are excluded in two phases: first based on screening criteria to exclude
128 models with lower value for the anticipated uses of the ensemble, and second using the method
129 of Cannon (2015) to represent the range of climate changes in the remaining models.

130 2.2.1 *Screening criteria*

131 Priority for exclusion from model subsets was established using four screening criteria.
132 The screening criteria are more subjective than the six selection criteria defined above. They
133 generally are not sufficient in isolation but combinations of the criteria provide some justification
134 for model exclusions.

- 135 • **Criterion 7. Constraints on equilibrium climate sensitivity (ECS).** Multiple lines of
136 evidence indicate that the Earth's equilibrium climate sensitivity (ECS) is *likely*
137 (probability > 66%) between 2.5°C and 4°C and *very likely* ($p > 90\%$) between 2°C and
138 5°C (Sherwood et al. 2020, Arias et al. 2021). The evidence is robust for the lower bound,
139 and weaker for the upper bound. From one perspective, inclusion of models with ECS
140 outside this very likely range biases the multi-model ensemble mean and unnecessarily
141 increases the modeling uncertainty in downstream analyses (Ribes et al. 2021). An
142 alternate perspective is that high-sensitivity models are useful as a representation of high-
143 impact, low-likelihood scenarios (Sutton and Hawkins 2020). To accommodate both
144 perspectives, we provide structured subsets with and without high-sensitivity models.
- 145 • **Criterion 8. Model resolution.** Some ScenarioMIP models have sufficiently high spatial
146 resolution to resolve macrotopography, e.g., to differentiate the major mountain ranges of
147 the Western Cordillera. These models are weighted towards inclusion in the ordered

148 subsets. Models with very low spatial resolution are weighted towards exclusion in the
149 subset.

150 • **Criterion 9. Number of simulation runs.** The ensemble is designed for analysis of
151 projected climate normals; the climate change signal is of primary interest. In this
152 context, internal variability of the models is a confounding factor, producing erratic
153 climate change trajectories in noisy climate variables like precipitation and winter
154 temperature. The signal-to-noise ratio can be increased by averaging the projected
155 normals over multiple simulations of the same emissions scenario. Models with only one
156 run are weighted for exclusion.

157 • **Criterion 10: Grid cell artefacts.** Models exhibiting spatially anomalous climate
158 changes in individual grid cells are problematic for many of the intended uses of this
159 ensemble, and are weighted for exclusion from the structured subsets.

160 2.2.2 *Ordered subsets*

161 After exclusion of models using the screening criteria above, an order of exclusion for the
162 remaining models is defined using the Katsavounidis–Kuo–Zhang (KKZ) algorithm, using the
163 application to climate model ensemble selection described by Cannon (2015). KKZ
164 deterministically selects models that best represent the spread of multivariate climate changes
165 projected by the ensemble. KKZ subset selection is ordered, starting with the model closest to
166 the ensemble centroid, and incrementally adding models to a region of the ensemble variation
167 that is poorly represented by each successive subset.

168 Since the spatial patterns of climate change differ among models, we provide separate
169 KKZ subsets for each of the seven IPCC climate reference regions (Iturbide et al. 2020) within
170 North America. We also provide an ordered subset for North America as a whole, but caution
171 that ensembles of less than 8 models are likely insufficient to represent spatial variation in
172 modeling uncertainty at continental scales (Pierce et al. 2009, McSweeney et al. 2014, Cannon
173 2015). The implementation of KKZ in this study used the mean of the z-standardized seasonal
174 changes in T_{\min} , T_{\max} , and precipitation in four consecutive 20-year time periods starting with
175 2021-2040 and three emissions scenarios (SSP1-2.6, SSP2-4.5, and SSP3-7.0).

176 2.3 *Analysis of model bias*

177 We assessed model bias as *mean absolute bias* over North America in each monthly
178 climate variable. For each grid cell, i , the mean simulated 1961-1990 climate normal of the K
179 historical model runs, f_{ik} is calculated as

$$\bar{f}_i = \frac{1}{K} \sum_{k=1}^K f_{ik} \quad (1)$$

180 The absolute value of the difference between the simulated 1961-1990 normal, \bar{f}_i , and the
181 observed 1961-1990 normal, o_i , aggregated onto the native model grid is calculated for each grid
182 cell:

$$|e_i| = |\bar{f}_i - o_i| \quad (2)$$

183 The mean absolute bias, $|e|$, over all N projected grid cells in North America is calculated as:

$$|e| = \frac{1}{N} \sum_{i=1}^N |e_i| \quad (3)$$

184 To equalize the area of grid cells, we projected absolute bias in the native model grid onto a
185 Lambert Conformal Conic grid with 0.5° resolution prior to calculating this mean.

186 For precipitation variables, Equations 1 and 2 were performed on log-transformed normals.
187 Subsequent to Equation 3, this log-transformation was reversed by taking the exponent of
188 absolute bias. Doing so expresses absolute bias of precipitation as a factor of magnitude. e.g.,
189 simulated precipitation normals of 50% and 200% relative to observed precipitation both have an
190 absolute bias of 2.

191 **2.4 Cluster analysis**

192 For visualization of similarity among models, we perform a standard cluster analysis on six
193 climate variables (minimum temperature, maximum temperature, and precipitation for winter
194 and summer) at approximately 400 locations (by resampling all models to a common 300 km
195 resolution). To reduce dimensions for clustering, we used three principal components instead of
196 the original six variables, resulting in 1200 variables for the construction of the dendrogram (400
197 locations x 3 principal climate components). We used Ward's hierarchical clustering algorithm
198 with a Euclidean distance of standardized principal components (i.e., a Mahalanobis distance
199 metric), implemented with the hclust package for the R programming environment.

200 **3 Results**

201 **3.1 Ensemble selection**

202 There were 44 models in the CMIP6 ScenarioMIP holdings as of December 15, 2020
203 (Table 1). Twelve of these candidates were excluded because they did not provide monthly
204 means of T_{\min} and T_{\max} (Criterion 1). Notably, CESM2 does provide T_{\min} and T_{\max} in its future
205 projections, but due to an archiving error these variables are not available for historical runs. An
206 additional eleven models were excluded because they had less than three historical runs
207 (Criterion 2) or an incomplete scenario set (Criterion 3). Of the 21 models that passed these first
208 three strict criteria, we excluded two more models on the basis of having a clear choice between
209 models from the same institution (Criterion 4): CanESM5-CanOE in favour of CanESM5; and
210 EC-Earth3-Veg in favour of EC-Earth3. In addition, of the several variants of the GISS-E2-1-G
211 model, we selected the r*i1p3f1 variant because it had the most complete set of scenario
212 simulations. We downloaded historical simulations from the remaining 19 models for further
213 evaluation. For practical purposes, we limited downloads to 5 historical simulations for EC-
214 Earth3 due to its relatively high resolution, and 10 simulations for other models.

215 To assist with choosing among models from the same institution (Criterion 4) or with
216 shared components (Criterion 5), we conducted an analysis of bias in T_{\min} , T_{\max} , and

217 precipitation (PPT) (Figure 1). We excluded AWI-CM-1-1-MR on the sole basis of its very high
218 temperature bias (Criterion 6). NESM3 also has high bias relative to the other models, and
219 excluded due to shared components with MPI-ESM1 (Criterion 5). None of the other related
220 models were distinct from each other in terms of bias.

221 Final choices from among related models were: UKESM1.0-LL selected over HadGEM3-
222 GC31-LL due to higher resolution and more simulations; MIROC6 over MIROC-ES2L due to
223 higher number of runs and regionally high biases in the Pacific Northwest; MPI-ESM1.2-HR
224 over MPI-ESM1-2-LR to improve representation of high-resolution models in the ensemble; and
225 CNRM-ESM2-1 arbitrarily selected over CNRM-CM6-1 in favour of the ESM configuration. In
226 summary, the six criteria reduced the 44 candidate models to a 13-model ensemble (Table 2).

227 **Table 1: Candidate models, model exclusion criteria, and number of simulation runs.** Model list and
 228 number of simulations per scenario are ESGF holdings as of December 15, 2020. ECS is equilibrium
 229 climate sensitivity (long-term temperature change in response to an instant doubling of CO₂); ECS values
 230 are quoted from Meehl et al. (2020). See Table 1 for citations and institutions of selected models.

Model	Criterion for exclusion	ECS	ESGF holdings					Analyzed				
			historical	ssp126	ssp245	ssp370	ssp585	historical	ssp126	ssp245	ssp370	ssp585
ACCESS-CM2	2 <3 historical runs	4.7	2	1	1	1	1					
ACCESS-ESM1-5		3.9	30	10	30	10	10	10	10	10	10	10
AWI-CM-1-1-MR	6 very high bias	3.2	5	1	1	5	1	3				
BCC-CSM2-MR		3.3	3	1	1	1	1	3	1	1	1	1
CAMS-CSM1-0	1 No tmax/tmin	2.3	3	2	2	2	2					
CESM2	1 No tmax/tmin in historical	5.2	11	3	3	3	3					
CESM2-WACCM	1 No tmax/tmin in historical	4.8	3	1	5	3	5					
CIESM	3 incomplete scenarios		3	1			1					
CMCC-CM2-SR5	1 No tmax/tmin		1	1	1	1	1					
CNRM-CM6-1	4 same institution	4.9	30	6	10	6	6	10				
CNRM-CM6-1-HR	2 <3 historical runs	4.3	1	1	1	1	1					
CNRM-ESM2-1		4.8	11	5	10	5	5	11	5	5	5	5
CanESM5		5.6	65	50	50	50	50	10	10	10	10	10
CanESM5-CanOE	4 same institution		3	3	3	3	3					
E3SM-1-1	3 incomplete scenarios	5.3	1				1					
EC-Earth3		4.3	73	7	30	7	58	5	5	5	5	5
EC-Earth3-AerChem	2 <3 historical runs		2			1						
EC-Earth3-Veg	4 same institution	4.3	8	7	8	6	6					
FGOALS-f3-L	1 No tmax/tmin	3	3	3	3	3	3					
FGOALS-g3	1 No tmax/tmin	2.9	6	4	4	5	4					
FIO-ESM-2-0	3 incomplete scenarios		3	3	3		3					
GFDL-CM4	3 incomplete scenarios	3.9	1		1		1					
GFDL-ESM4		2.7	3	1	3	1	1	3	1	3	1	1
GISS-E2-1-G	selected r*i1p3f1 variants	2.7	47	7	30	19	7	4	4	4	4	4
HadGEM3-GC31-LL	5 shared components (UKESM1)	5.6	5	1	4		4	4				
HadGEM3-GC31-MM	3 incomplete scenarios	5.4	4	1			4					
IITM-ESM	1 No tmax/tmin		1	1	1	1	1					
INM-CM4-8	2 <3 historical runs	1.8	1	1	1	1	1					
INM-CM5-0		1.9	9	1	1	5	1	9	1	1	5	1
IPSL-CM6A-LR		4.6	9	5	6	9	5	9	5	6	9	5
KACE-1-0-G	1 No tmax/tmin		3	3	3	3	3					
KIOST-ESM	2 <3 historical runs		1	1	1		1					
MCM-UA-1-0	1 No tmax/tmin		2	1	1	1	1					
MIROC-ES2L	4 same institution	2.7	3	3	3	3	3	3				
MIROC6		2.6	50	50	50	3	50	10	10	10	3	10
MPI-ESM-1-2-HAM	3 incomplete scenarios		3			2						
MPI-ESM1-2-HR		3	10	2	2	10	2	8	2	2	10	1
MPI-ESM1-2-LR	4 same institution	3	10	10	10	10	10	10				
MRI-ESM2-0		3.1	7	1	5	5	2	5	1	5	1	1
NESM3	5 shared components (MPI-ESM1)	4.8	5	2	2		2	5				
NorESM2-LM	1 No tmax/tmin	2.6	3	1	3	3	1					
NorESM2-MM	1 No tmax/tmin	2.5	1	1	2	1	1					
TaiESM1	1 No tmax/tmin	4.4	2	1	1	1	1					
UKESM1-0-LL		5.4	19	16	17	16	5	10	5	5	5	5

231
232

233 **Table 2: Institution and citation for each model in the 13-model ensemble.**

Model	Institutions	Citation
ACCESS-ESM1.5	Commonwealth Scientific and Industrial Research Organisation (Australia)	Ziehn et al. (2020)
BCC-CSM2	Beijing Climate Center (China)	Wu et al. (2019)
CanESM5	Canadian Centre for Climate Modelling and Analysis (Canada)	Swart et al. (2019)
CNRM-ESM2-1	CNRM (Centre National de Recherches Meteorologiques) and CERFACS (Centre Europeen de Recherche et de Formation Avancee en Calcul Scientifique) (France)	Séférian et al. (2019)
EC-Earth3	EC-Earth Consortium (European Community)	Döscher et al. (2021)
GFDL-ESM4	National Oceanic and Atmospheric Administration, Geophysical Fluid Dynamics Laboratory (USA)	Dunne et al. (2020)
GISS-E2.1	Goddard Institute for Space Studies (USA)	Kelley et al. (2020)
INM-CM5.0	Institute for Numerical Mathematics (Russia)	Volodin et al. (2017)
IPSL-CM6A-LR	Institut Pierre Simon Laplace (France)	Boucher et al. (2020)
MIROC6	JAMSTEC (Japan Agency for Marine-Earth Science and Technology), AORI (Atmosphere and Ocean Research Institute), NIES (National Institute for Environmental Studies), and R-CCS (RIKEN Center for Computational Science) (Japan)	Tatebe et al. (2018)
MPI-ESM1.2-HR	Max Planck Institute for Meteorology (Germany)	Müller et al. (2018)
MRI-ESM2.0	Meteorological Research Institute (Japan)	Yukimoto et al. (2019)
UKESM1	Met Office Hadley Centre and Natural Environment Research Council (UK)	Sellar et al. (2019)

234

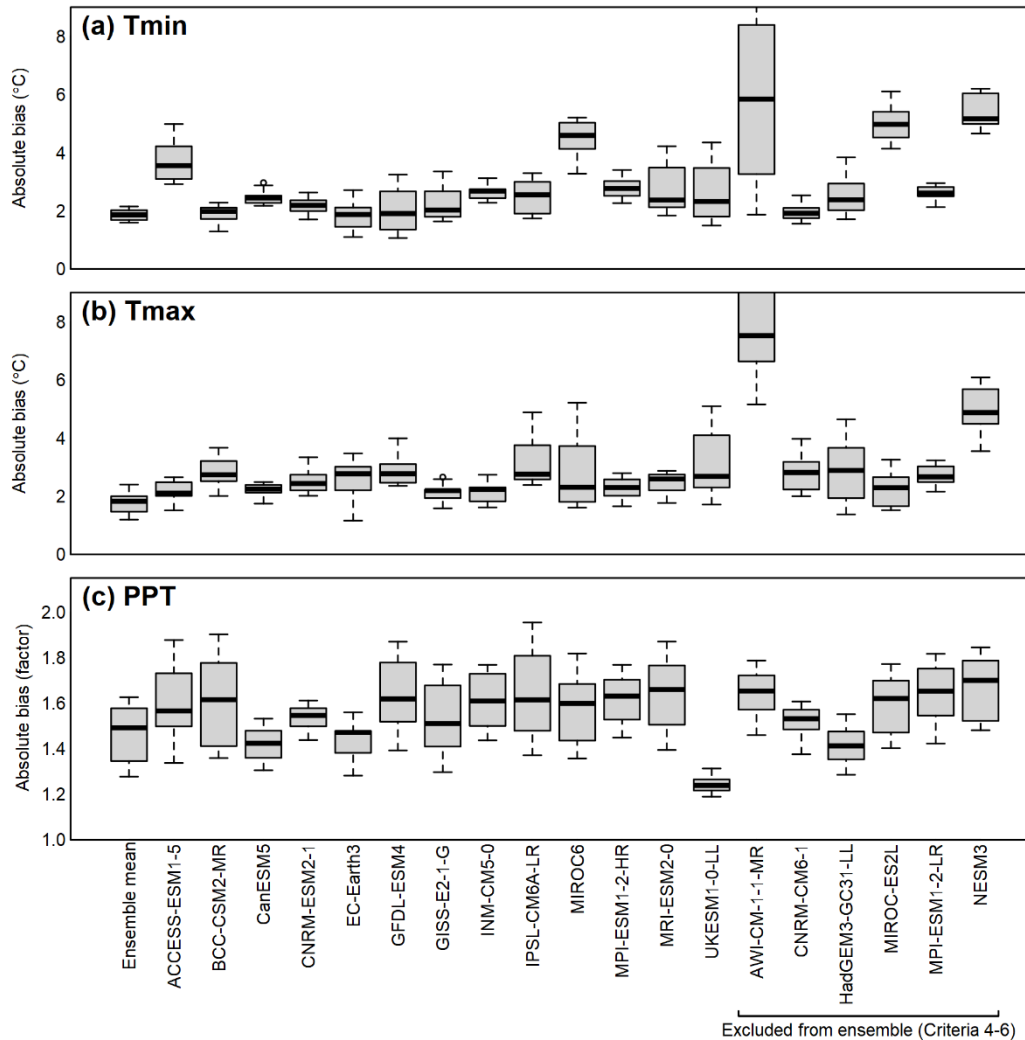
235 **3.2 Attributes of the 13-model ensemble**

236 **3.2.1 Representation of the full CMIP6 ensemble**

237 The 13-model ensemble has a mean global equilibrium climate sensitivity (ECS) of 3.7°C
 238 and a range of 1.9-5.6°C, which matches ECS of the full CMIP6 ensemble (3.7°C; 1.8-5.6°C)
 239 (Meehl et al. 2020).

240 **3.2.2 Model bias**

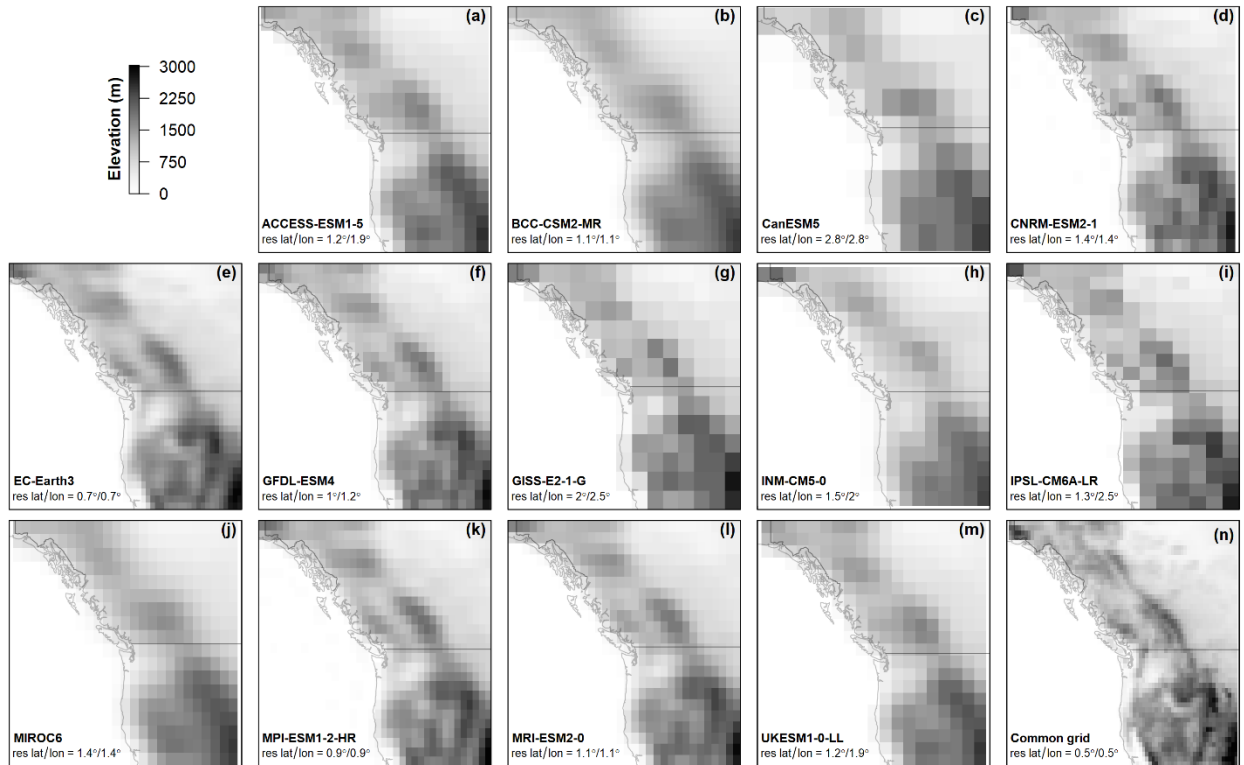
241 The ensemble mean has a mean absolute bias of 2°C in T_{\min} and T_{\max} . Most models have
 242 biases similar to this baseline. However, AWI-CM-1-1-MR has exceptionally high bias in both
 243 T_{\min} and T_{\max} . ACCESS-ESM1.5, MIROC6, MIROC-ES2L and NESM3 also have high biases in
 244 T_{\min} and/or T_{\max} . There is less differentiation in precipitation biases among models and with the
 245 ensemble mean. UKESM1, CanESM5, EC-Earth3, and HadGEM3-GC31 have lower
 246 precipitation biases than the ensemble mean.



247
 248 **Figure 1: Model biases in monthly means of (a) daily minimum temperature, (b) daily maximum**
 249 **temperature, and (c) precipitation.** Each box represents 12 values of mean absolute bias over North
 250 America, one for each month. Absolute bias for precipitation is expressed as a factor of magnitude, e.g.,
 251 relative biases of 50% and 200% both have an absolute bias of 2.

252 3.2.3 Spatial resolution and model orography

253 The selected 13-model ensemble has a mean latitudinal grid resolution of 1.4° (range of
 254 0.7° - 2.8°) (Figure 2). Four models (EC-Earth3, GFDL-ESM4, MPI-ESM1.2-HR, and MRI-
 255 ESM2.0) resolve the macrotopography of the Western Cordillera, namely the Sierra Nevada,
 256 Cascade Range, Rocky Mountains, and British Columbia Coast Ranges. BCC-CSM2-MR does
 257 not resolve these ranges, despite having sufficient grid resolution to do so. CanESM5 has a very
 258 low resolution of $2.8^\circ \times 2.8^\circ$.



259
 260 **Figure 2: Effective topographic resolution of the 13 selected models.** (a-m) model orography
 261 (elevation of land surface) in the native grid of each model. The extent of the map is central-western
 262 North America (106-142°W, 37-62°N). The common grid (panel n) is the 0.5° grid used for extraction of
 263 observations from ClimateNA.

264 3.2.4 Projected climate change

265 A visual comparison of projected seasonal changes in T_{\min} , T_{\max} , and PPT (Figure 3)
 266 indicates some basic attributes of the ensemble simulations. All models exhibit Arctic
 267 amplification of winter temperatures, though it is relatively subtle in EC-Earth3. Most models
 268 project the strongest summer warming at mid-latitudes. All models, with the exception of
 269 UKESM1, have a similar pattern of warming in T_{\min} and T_{\max} , though the magnitude of warming
 270 is greater for T_{\min} in most models.

271 Continental-scale patterns of winter (Dec-Feb) precipitation change are somewhat
 272 consistent among models, with declines in Mexico and increases in the Arctic regions.
 273 Deviations from this pattern are strongest in models with few (1-3) historical runs for SSP2-4.5
 274 (BCC-CSM2-MR, GFDL-ESM4 and INM-CM5.0), and are likely due to internal variability.
 275 This result indicates the benefit of multiple runs in smoothing out natural variability to reveal the
 276 anthropogenic climate change signal in noisy climate variables like precipitation and winter
 277 temperature.

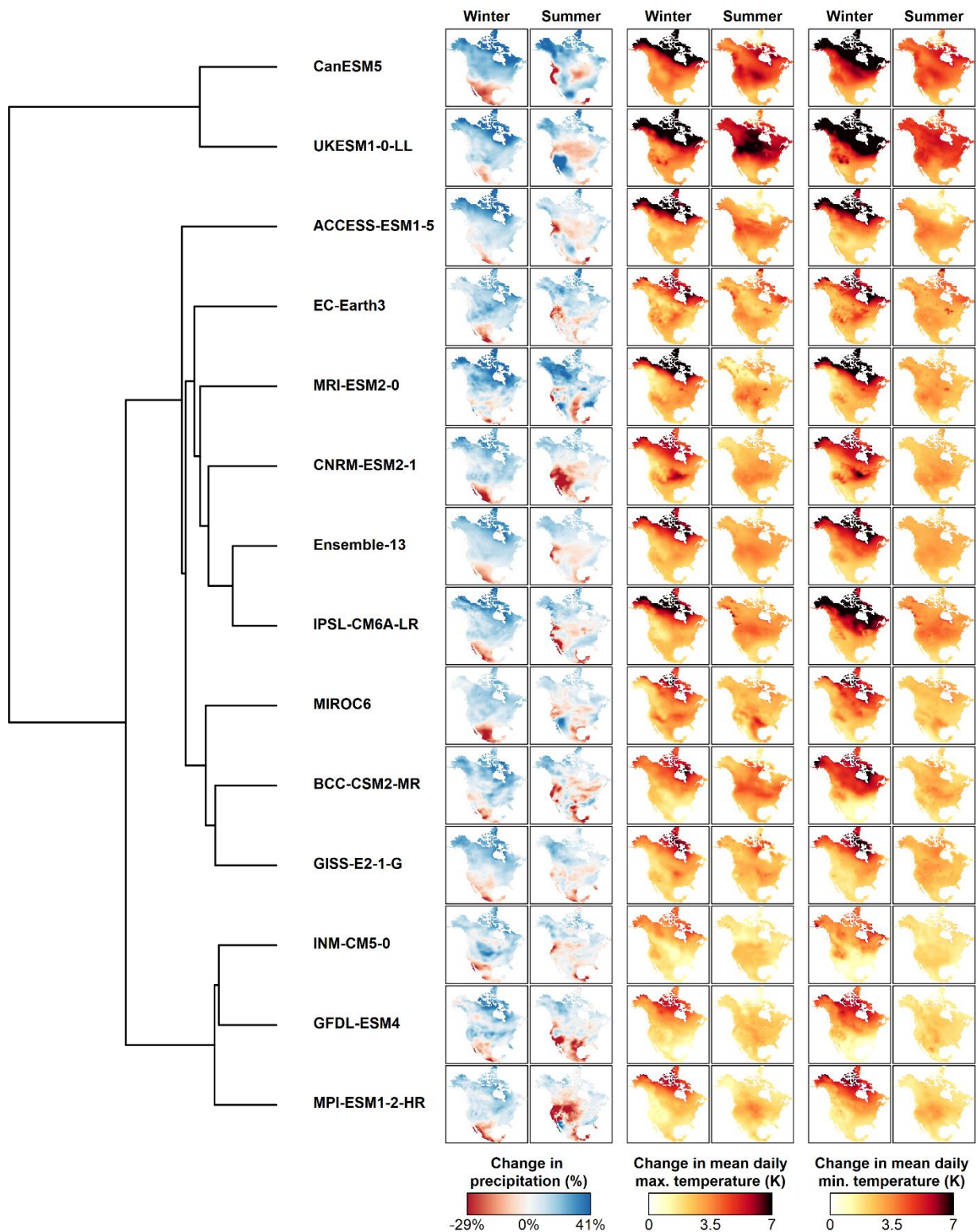
278 Most models project a reduction in summer (Jun-Aug) precipitation in the coastal areas of
 279 the Pacific Northwest (California, Oregon, Washington, and southern British Columbia). There
 280 is substantial disagreement among models in summer precipitation change over the rest of the
 281 continent. The muted summer precipitation change in the ensemble mean hides this ensemble

282 disagreement, and underscores the importance of assessing climate change impacts with an
283 ensemble of model projections rather than solely using the ensemble mean.

284 The two high-ECS models CanESM5 and UKESM1 have similar patterns and magnitudes
285 of change in winter temperature and precipitation. However, they differ substantially in the
286 summer, with UKESM1 showing much higher increases in daytime temperatures (T_{\max}) in
287 Temperate and Boreal regions and stronger declines in precipitation in Central North America.
288 Although CanESM5 has a higher ECS and stronger trend in 1970-2014 global heating (Liang et
289 al. 2020), UKESM1 projects stronger mid-century heating over North America.

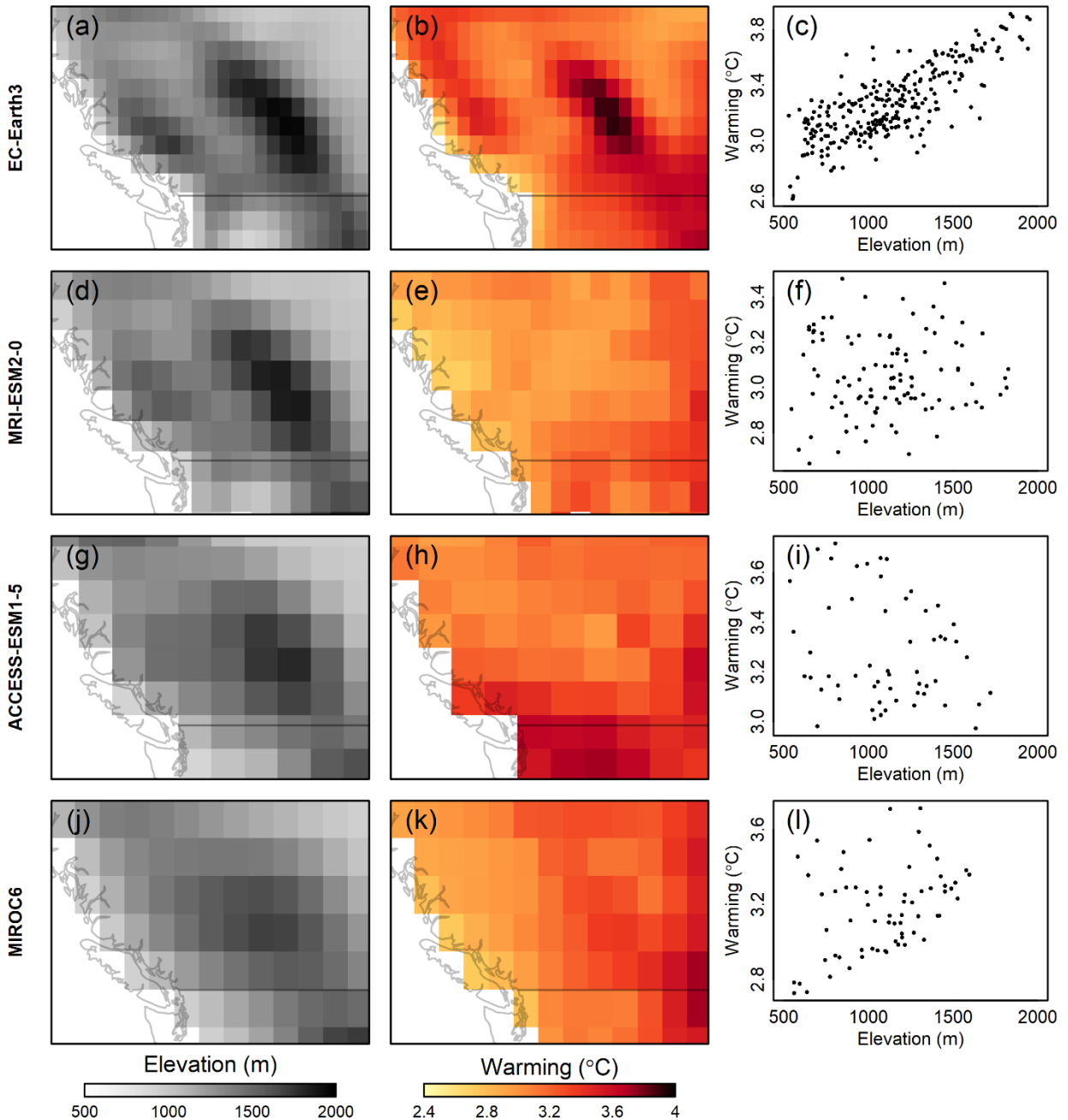
290

291



292 **Figure 3: Spatial variation in climate change responses among the 13-model ensemble.** Mapped
 293 climate changes are for the mean projected climate of the 2041-2060 period (SSP2-4.5). Precipitation is
 294 log-scaled to provide proportional magnitude of positive and negative changes. Models are structured by
 295 a cluster dendrogram of spatial similarity in seasonal climate changes in all three climate elements.

317 adjacent plateaus (Figure 5b,c). In contrast, MRI-ESM2.0 exhibits no relationship between
 318 elevation and warming (Figure 5e,f). ACCESS-ESM1.5 and MIROC6 represent the mountain
 319 ranges as a single feature in their model orography. ACCESS-ESM1.5 exhibits a weak negative
 320 relationship of warming to elevation, and MIROC6 exhibits a weak positive relationship.

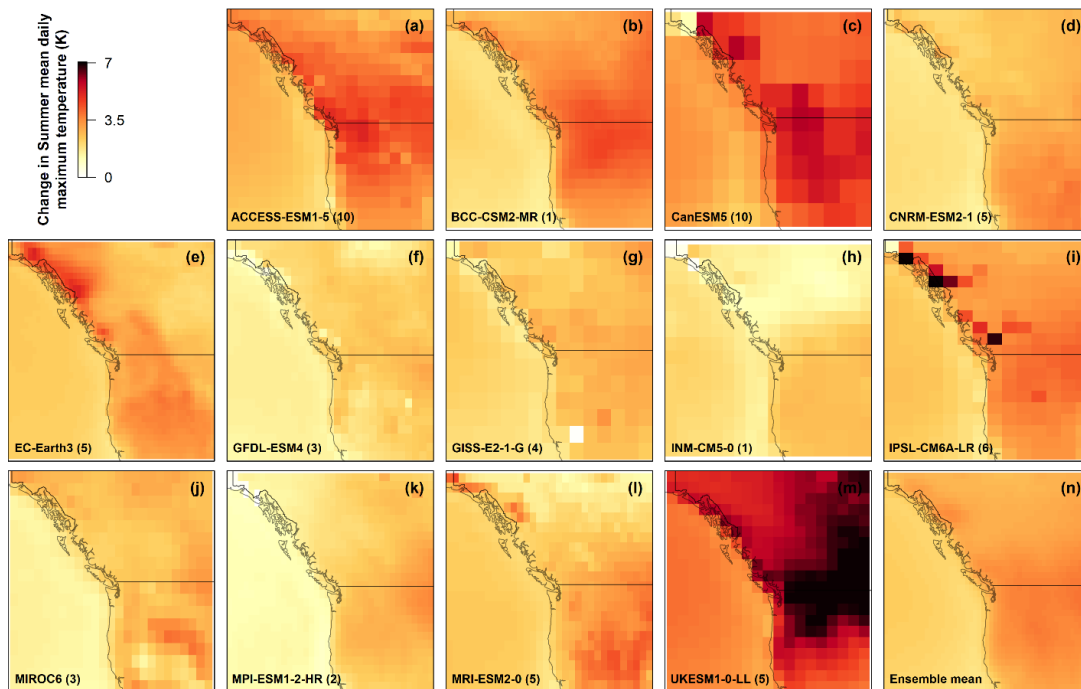


321
 322 **Figure 5: Relationships between elevation and warming (autumn Tmax) over southwestern Canada**
 323 **in four CMIP6 models.** To emphasize spatial variation within each model rather than warming
 324 magnitude among models, warming for each model is selected from different periods: 2041-2060 for EC-
 325 Earth3 and ACCESS-ESM1.5; 2061-2080 for MRI-ESM2.0; and 2081-2100 for MIROC6. Projected
 326 warming is under SSP2-4.5 for all models. Coastal cells (elevation <500m) are excluded to reduce the
 327 maritime influence on the analysis.

328 **3.3 Ensemble subset selection**

329 **3.3.1 Screening exclusions**

330 The following models are prioritized for exclusion from subsets of the ensemble based on
331 combinations of the four screening criteria: **CanESM5**, because its very high climate sensitivity
332 (ECS 5.6°C) is also represented by UKESM1.0-LL and because its very low horizontal
333 resolution is less suitable for downscaling; **INM-CM5.0**, because it has very low climate
334 sensitivity (ECS 1.9°C) and is an outlier among CMIP6 models for under-representing the
335 observed 1975-2014 global temperature trend (Liang et al. 2020) (Criterion 7). In addition, this
336 model has only one simulation for most scenarios, producing a less robust climate signal
337 (Criterion 9); **BCC-CSM2-MR**, due to having a single simulation for each scenario (Criterion 9)
338 and low topographic resolution (Criterion 8); and **IPSL-CM6A-LR**, due to isolated grid cells
339 with very high summer warming in the BC Coast Ranges and Southeast Alaska (Figure 6;
340 Criterion 10). The warming in these cells may be physically plausible in the model's simplified
341 topography, but is problematic for downscaling to higher spatial resolutions.



342 **Figure 6: Summer daytime warming in the 13-model ensemble over central-western North America**
343 **(106-142W, 37-62N).** Values are the change in summer T_{\max} for the 2041-2060 period (SSP2-4.5),
344 relative to 1961-1990, in the native model grid. Change is calculated from the mean of multiple
345 simulation runs per model, specified next to the model name.
346

347 UKESM1 also has very high climate sensitivity, similar to CanESM5, that is assessed as
348 very unlikely based on observational evidence (Sherwood et al. 2020, Arias et al. 2021). Some
349 researchers may wish to constrain their ensemble subset to observations by excluding this model.
350 Others may wish to include a high-sensitivity model in their subset as a representation of the
351 long tail of uncertainty in the upper limit of climate sensitivity (Sutton 2018). To accommodate
352 both perspectives, we provide structured subsets with and without UKESM1 in the ordered
353 ensemble subsets. We preferred UKESM1 over CanESM5 as a representative of high-sensitivity

354 models due to its higher grid resolution and closer alignment with the observed post-1970 global
 355 heating trend (Liang et al. 2020).

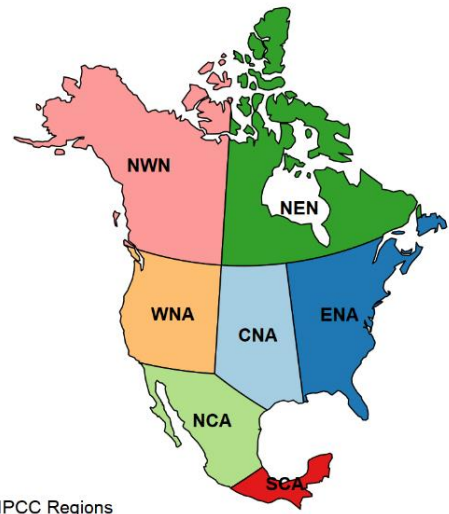
356 The 8-model subset has a mean global ECS of 3.4°C (2.6-4.8°C). The 9-model subset that
 357 includes UKESM1 has a mean global ECS of 3.6°C (2.6-5.4°C), using ECS values provided by
 358 Meehl et al. (2020).

359 **3.3.2 Ordered subsets**

360 Table 3 specifies ordered subsets of the models that passed screening criteria 7-10. For a
 361 desired region and subset size, the ensemble subset for each region includes all models listed at
 362 and above the desired subset size. For example, a 4-model ensemble for the NEN region would
 363 include CNRM-ESM2-1, UKESM1.0-LL, EC-Earth3, and MPI-ESM1.2-HR. The considerable
 364 variation among regions in the order of the subsets underscores the spatial variation in climate
 365 change responses across North America. The exception to this variation in model order is that
 366 UKESM1 is the second model in all regions. Since the first position in the order is the model
 367 closest to the ensemble centroid and the second position is the model furthest from the centroid,
 368 this result indicates that UKESM1 consistently projects the most extreme climate changes
 369 throughout the continent.

Table 3: Ordered subsets of the 13-model ensemble. Subsets are provided for North America (NAM) and the 7 IPCC reference regions (Figure 7). Model abbreviations are ACC (ACCESS-ESM1.5), CNRM (CNRM-ESM2-1), EC (EC-Earth3), GFDL (GFDL-ESM4), GISS (GISS-E2-1-G), MIR (MIROC6), MPI (MPI-ESM1.2-HR), MRI (MRI-ESM2.0), and UK (UKESM1.0-LL). Exclusion of UKESM1 provides an ensemble that is consistent with assessed constraints on equilibrium climate sensitivity.

Subset size	IPCC Reference Region							
	NEN	NWN	WNA	CNA	ENA	NCA	SCA	NAM
Including UKESM1-0-LL								
1	CNRM	CNRM	MRI	ACC	EC	MRI	MRI	CNRM
2	UK	UK	UK	UK	UK	UK	UK	UK
3	EC	MPI	MPI	MPI	MPI	GFDL	GFDL	MPI
4	MPI	EC	GISS	CNRM	MRI	MIR	MIR	MRI
5	MRI	ACC	MIR	MIR	MIR	EC	EC	EC
6	ACC	MRI	CNRM	GISS	GFDL	MPI	MPI	MIR
7	GFDL	MIR	GFDL	EC	ACC	CNRM	CNRM	ACC
8	GISS	GISS	EC	GFDL	GISS	ACC	ACC	GISS
9	MIR	GFDL	ACC	MRI	CNRM	GISS	GISS	GFDL
Excluding UKESM1-0-LL								
1	CNRM	CNRM	MRI	MRI	GISS	GISS	GISS	CNRM
2	EC	EC	MPI	MPI	GFDL	EC	EC	MPI
3	MPI	ACC	GISS	CNRM	MRI	MRI	MRI	EC
4	MRI	MPI	MIR	MIR	ACC	MIR	MIR	MRI
5	ACC	MIR	CNRM	EC	CNRM	GFDL	GFDL	ACC
6	GISS	GISS	EC	GFDL	EC	CNRM	CNRM	GISS
7	GFDL	MRI	GFDL	GISS	MPI	ACC	ACC	MIR
8	MIR	GFDL	ACC	ACC	MIR	MPI	MPI	GFDL



IPCC Regions
Figure 7: IPCC reference regions (Iturbide et al. 2020) used for ordered subsets of the ensemble.

370 4 Discussion

371 We selected 13 CMIP6 models from a candidate pool of 44 models contributing to the
372 CMIP6 experiment. This 13-model ensemble is representative of the distribution of equilibrium
373 climate sensitivity in the full CMIP6 ensemble. The 13-model ensemble facilitates robust
374 downscaling by using multiple simulations per scenario for each model and excluding models
375 with high bias. We provided rationale for an 8-member subset of the ensemble based on
376 screening criteria and order these 8 models for selection of smaller ensembles for regional
377 analysis in North America. We also highlighted some tradeoffs among the models in terms of
378 grid resolution, number of simulation runs, climate sensitivity, regional biases, and local
379 artefacts. These results, and the accompanying web application ([https://bcgov-
380 env.shinyapps.io/cmip6-NA/](https://bcgov-env.shinyapps.io/cmip6-NA/)), help readers to make model selections appropriate to their specific
381 research objectives.

382 4.1 Model bias

383 The bias assessment was a useful way to identify models with extreme divergence from the
384 observed climate. High biases were the sole basis for the exclusion of one model, AWI-CM1-1-
385 1-MR, and are an attribute of concern in two of the models selected for the ensemble, ACCESS-
386 ESM1.5 and MIROC6. The moderate biases in the rest of the ensemble, however, do not
387 necessarily indicate a problem with the models. Bias is the difference between model
388 simulations and the observed climate. We controlled the confounding influence of natural
389 variability in each model by calculating bias using the mean of several simulation runs. This
390 measure is not possible for observations since there is only one realization of the observed
391 climate. Natural variability in the observed climate, therefore, could produce apparent biases
392 even in a hypothetical “perfect” model (Lanzante et al. 2018). The ensemble mean absolute bias
393 of 2°C in temperature and by a factor of 1.5 in precipitation cannot be definitively attributed to
394 the models or the ensemble; it is to some extent an artefact of natural variability in the observed
395 climate.

396 4.2 Grid resolution

397 Four of the models in the ensemble have horizontal grid resolution sufficient to resolve
398 major mountain ranges. One model (EC-Earth3) has relatively high resolution (0.7°x0.7°)
399 approaching the previous generation of regional climate models used for dynamical downscaling.
400 The trend towards higher resolution is encouraging, but the benefits of moderate resolution
401 models for km-scale downscaling are ambiguous. On one hand, resolving mountain ranges
402 allows for stronger differentiation of maritime/continental transitions (Lanzante et al. 2018),
403 windward and leeward dynamics (Kanehama et al. 2019), and elevation-dependent climate
404 changes (Palazzi et al. 2019). On the other hand, these resolved mountain ranges are still highly
405 simplified features in even the highest resolution models in the ensemble. Resolved high-
406 elevation processes such as enhanced warming due to snow albedo feedbacks (Salathé et al.
407 2008) will be applied to unresolved low-elevation locations (e.g., valleys) during change-factor
408 downscaling. Hence, higher-resolution models offer new insights, but also introduce new
409 problems for statistical downscaling. In the absence of additional downscaling measures to
410 address these problems, we do not view the higher-resolution models in the ensemble as

411 intrinsically more valuable or valid. They do, however, make a distinct contribution and the
412 range of grid resolution in the ensemble improves the representation of modeling uncertainties.

413 **4.3 Diurnal temperature range**

414 Underestimation of DTR is a persistent feature of climate models (Wang and Clow 2020).
415 Intermodel differences in DTR can be attributed to differences in parameterizations for clouds,
416 aerosols and soil moisture, among others (Lindvall and Svensson 2015). However, the consistent
417 underestimation of DTR relative to observations has not been definitively explained. Part of the
418 underestimation of DTR may be due to differences in the timescale of DTR measurement in
419 observations and models; since T_{\min} and T_{\max} are measured instantaneously in observations but
420 simulated over longer timesteps in models, models are expected to have lower DTR (Wilson et
421 al. 2008, Rupp et al. 2013). To the extent that underestimation of DTR is an artefact of the
422 different timescales of measurement in observations and models, rather than of systematic biases
423 in the driving processes, some overestimation of T_{\min} and underestimation of T_{\max} can be
424 expected even from a perfect model.

425 **4.4 Reconciling the equilibrium climate sensitivity of the ensemble with observational** 426 **constraints**

427 The 13-model ensemble selected here, like the full CMIP6 ensemble, has a mean (3.7 °C)
428 and upper limit (5.6°C) of equilibrium climate sensitivity that substantially exceeds the IPCC
429 AR6 assessed best estimate ECS of 3°C and *very likely* upper limit of 5°C (Arias et al. 2021). In
430 other words, the 13-model ensemble contains models that simulate stronger global warming than
431 is supported by multiple lines of observational evidence. Five (38%) of the 13 models are above
432 the IPCC AR6 assessed *likely* upper limit on ECS of 4 °C, and two (15%) of the models are
433 above the *very likely* upper limit of 5°C. If the ensemble were to strictly conform to the IPCC
434 assessed range, there would be only two models exceeding 4 °C ECS and no models exceeding
435 5°C, following the IPCC’s probabilistic definitions of *likely* (one-sided $p>83\%$) and *very likely*
436 (one-sided $p>95\%$).

437 The need to reconcile the CMIP ensemble ECS range with observational constraints is a
438 new dilemma for climate change impacts and adaptation researchers. It is long been agreed that
439 model democracy (one model, one vote) is not a strictly valid method of assessing climate
440 change uncertainty (Knutti 2010, Leduc et al. 2016). However, in the past this objection was
441 somewhat academic since the distribution of ECS in CMIP ensembles approximately matched
442 the (wider) range of ECS supported by other lines of evidence. For practical purposes it was
443 reasonable for analysts to use the multimodel ensemble spread in previous CMIP generations as
444 a proxy for scientific uncertainty on climate change. This approach is no longer valid given the
445 incongruence between the CMIP6 ensemble range of ECS and the IPCC assessed range. Careful
446 model selection is now required to avoid biasing regional climate change analyses.

447 There are several viable approaches to constrain CMIP6 ensembles in downscaled regional
448 analyses. Weighting the models based on observational constraints is possible for regional
449 analyses (Ribes et al. 2021). However, in practice many analyses will require simply selecting a
450 subset of the CMIP6 ensemble that is closer to the IPCC assessed range, as we have done with
451 the 8-model subset. The disadvantage of this approach is that it discards valuable information

452 from the excluded models. The CanESM5 and UKESM1 models are advanced models from
453 highly respected modeling centers, with demonstrated skill in modeling many Earth system
454 processes (Eyring et al. 2021). Further, these models have large ensembles of simulations for
455 each scenario (50 runs, in the case of CanESM5) which are useful for quantifying natural
456 variability. Expressing variables of interest relative to the amount of regional or global warming
457 is a widely practiced technique that facilitates inclusion of high-ECS models by removing the
458 timing of the warming as a factor in the ensemble spread. It is conceivable that both techniques
459 could be used in a single study; to use the 8-model ensemble for time-relevant analyses and a
460 larger ensemble for analyses where the warming level is more relevant. These considerations
461 highlight that the full CMIP6 ensemble is a somewhat arbitrary collection of non-independent
462 models, and careful ensemble selection is necessary to achieve a meaningful representation of
463 modeling uncertainty.

464 **5 Acknowledgements**

465 We acknowledge the World Climate Research Programme, which, through its Working
466 Group on Coupled Modelling, coordinated and promoted CMIP6. We thank the climate
467 modeling groups for producing and making available their model output, the Earth System Grid
468 Federation (ESGF) for archiving the data and providing access, and the multiple funding
469 agencies who support CMIP6 and ESGF.

470

471 **6 Literature Cited**

- 472 Arias, P. A., N. Bellouin, E. Coppola, R. G. Jones, G. Krinner, J. Marotzke, V. Naik, M. D.
473 Palmer, J. G-K. Plattner, Rogelj, M. Rojas, J. Sillmann, T. Storelvmo, P. W. Thorne, B.
474 Trewin, K. A. Rao, B. Adhikary, R. P. Allan, K. Armour, G. Bala, R. Barimalala, S. Berger,
475 J. G. Canadell, C. Cassou, A. Cherchi, W. Collins, W. D. Collins, S. L. Connors, S. Corti, F.
476 Cruz, F. J. Dentener, C. Dereczynski, A. Di Luca, A. D. Niang, F. J. Doblas-Reyes, A.
477 Dosio, H. Douville, F. Engelbrecht, V. Eyring, E. Fischer, P. Forster, B. Fox-Kemper, J. S.
478 Fuglestvedt, J. C. Fyfe, N. P. Gillett, L. Goldfarb, I. Gorodetskaya, J. M. Gutierrez, R.
479 Hamdi, E. Hawkins, H. T. Hewitt, P. Hope, A. S. Islam, C. Jones, D. S. Kaufman, R. E.
480 Kopp, Y. Kosaka, J. Kossin, S. Krakovska, J.-Y. Lee, J. Li, T. Mauritsen, T. K. Maycock,
481 M. Meinshausen, S.-K. Min, P. M. S. Monteiro, T. Ngo-Duc, F. Otto, I. Pinto, A. Pirani, K.
482 Raghavan, R. Ranasinghe, A. C. Ruane, L. Ruiz, J.-B. Sallée, B. H. Samset, S.
483 Sathyendranath, S. I. Seneviratne, A. A. Sörensson, S. Szopa, I. Takayabu, A.-M. Treguier,
484 B. van den Hurk, R. Vautard, S. Z. K. von Schuckmann, X. Zhang, and K. Zickfeld. 2021.
485 Technical Summary. Pages TS1-150 in V. Masson-Delmotte, P. Zhai, A. Pirani, S. L.
486 Connors, C. Péan, S. Berger, N. Caud, Y. Chen, L. Goldfarb, M. I. Gomis, M. Huang, K.
487 Leitzell, E. Lonnoy, J. B. R. Matthews, T. K. Maycock, T. Waterfield, O. Yelekçi, R. Yu,
488 and B. Zhou, editors. *Climate Change 2021: The Physical Science Basis. Contribution of*
489 *Working Group I to the Sixth Assessment Report of the Intergovernmental Panel on*
490 *Climate Change*. Cambridge University Press.
- 491 Boucher, O., J. Servonnat, A. L. Albright, O. Aumont, Y. Balkanski, V. Bastrikov, S. Bekki, R.
492 Bonnet, S. Bony, L. Bopp, P. Braconnot, P. Brockmann, P. Cadule, A. Caubel, F. Cheruy,
493 F. Codron, A. Cozic, D. Cugnet, F. D'Andrea, P. Davini, C. de Lavergne, S. Denvil, J.
494 Deshayes, M. Devilliers, A. Ducharne, J. L. Dufresne, E. Dupont, C. Éthé, L. Fairhead, L.
495 Falletti, S. Flavoni, M. A. Foujols, S. Gardoll, G. Gastineau, J. Ghattas, J. Y. Grandpeix, B.
496 Guenet, L. E. Guez, E. Guilyardi, M. Guimberteau, D. Hauglustaine, F. Hourdin, A.
497 Idelkadi, S. Joussaume, M. Kageyama, M. Khodri, G. Krinner, N. Lebas, G. Levvasseur,
498 C. Lévy, L. Li, F. Lott, T. Lurton, S. Luyssaert, G. Madec, J. B. Madeleine, F. Maignan, M.
499 Marchand, O. Marti, L. Mellul, Y. Meurdesoif, J. Mignot, I. Musat, C. Ottlé, P. Peylin, Y.
500 Planton, J. Polcher, C. Rio, N. Rochetin, C. Rousset, P. Sepulchre, A. Sima, D.
501 Swingedouw, R. Thiéblemont, A. K. Traore, M. Vancoppenolle, J. Vial, J. Vialard, N.
502 Viovy, and N. Vuichard. 2020. Presentation and Evaluation of the IPSL-CM6A-LR Climate
503 Model. *Journal of Advances in Modeling Earth Systems* 12:1–52.
- 504 Brunner, L., R. Lorenz, M. Zumwald, and R. Knutti. 2019. Quantifying uncertainty in European
505 climate projections using combined performance-independence weighting. *Environmental*
506 *Research Letters* 14:124010.
- 507 Cannon, A. J. 2015. Selecting GCM scenarios that span the range of changes in a multimodel
508 ensemble: Application to CMIP5 climate extremes indices. *Journal of Climate* 28:1260–
509 1267.
- 510 Cannon, A. J. 2018. Multivariate quantile mapping bias correction: an N-dimensional probability
511 density function transform for climate model simulations of multiple variables. *Climate*
512 *Dynamics* 50:31–49.

- 513 Döscher, R., M. Acosta, A. Alessandri, P. Anthoni, A. Arneth, T. Arsouze, T. Bergmann, R.
514 Bernadello, S. Bousetta, L.-P. Caron, G. Carver, M. Castrillo, F. Catalano, I. Cvijanovic, P.
515 Davini, E. Dekker, F. Doblas-Reyes, D. Docquier, P. Echevarria, U. Fladrich, R. Fuentes-
516 Franco, M. Gröger, J. v. Hardenberg, J. Hieronymus, M. P. Karami, J.-P. Keskinen, T.
517 Koenigk, R. Makkonen, F. Massonnet, M. Ménégos, P. Miller, E. Moreno-Chamarro, L.
518 Nieradzic, T. van Noije, P. Nolan, D. O'Donnell, P. Ollinaho, G. van den Oord, P. Ortega,
519 O. T. Prims, A. Ramos, T. Reerink, C. Rousset, Y. Ruprich-Robert, P. Le Sager, T.
520 Schmith, R. Schrödner, F. Serva, V. Sicardi, M. Sloth Madsen, B. Smith, T. Tian, E.
521 Tourigny, P. Uotila, M. Vancoppenolle, S. Wang, D. Wårlind, U. Willén, K. Wyser, S.
522 Yang, X. Yepes-Arbós, and Q. Zhang. 2021. The EC-Earth3 Earth System Model for the
523 Climate Model Intercomparison Project 6. *Geoscientific Model Development Discussions*
524 Preprint:1–90.
- 525 Dunne, J. P., L. W. Horowitz, A. J. Adcroft, P. Ginoux, I. M. Held, J. G. John, J. P. Krasting, S.
526 Malyshev, V. Naik, F. Paulot, E. Shevliakova, C. A. Stock, N. Zadeh, V. Balaji, C. Blanton,
527 K. A. Dunne, C. Dupuis, J. Durachta, R. Dussin, P. P. G. Gauthier, S. M. Griffies, H. Guo,
528 R. W. Hallberg, M. Harrison, J. He, W. Hurlin, C. McHugh, R. Menzel, P. C. D. Milly, S.
529 Nikonov, D. J. Paynter, J. Ploshay, A. Radhakrishnan, K. Rand, B. G. Reichl, T. Robinson,
530 D. M. Schwarzkopf, L. T. Sentman, S. Underwood, H. Vahlenkamp, M. Winton, A. T.
531 Wittenberg, B. Wyman, Y. Zeng, and M. Zhao. 2020. The GFDL Earth System Model
532 Version 4.1 (GFDL-ESM 4.1): Overall Coupled Model Description and Simulation
533 Characteristics. *Journal of Advances in Modeling Earth Systems* 12:e2019MS002015.
- 534 Eyring, V., S. Bony, G. A. Meehl, C. A. Senior, B. Stevens, R. J. Stouffer, and K. E. Taylor.
535 2016. Overview of the Coupled Model Intercomparison Project Phase 6 (CMIP6)
536 experimental design and organization. *Geoscientific Model Development* 9:1937–1958.
- 537 Eyring, V., N. P. Gillett, K. M. A. Rao, R. Barimalala, M. B. Parrillo, N. Bellouin, C. Cassou, P.
538 J. Durack, Y. Kosaka, S. McGregor, S. Min, O. Morgenstern, and Y. Sun. 2021. Human
539 influence on the climate system. Pages 1–202 *in* V. Masson-Delmotte, P. Zhai, A. Pirani, S.
540 L. Connors, C. Péan, S. Berger, N. Caud, Y. Chen, L. Goldfarb, M. I. Gomis, M. Huang, K.
541 Leitzell, E. Lonnoy, J. B. R. Matthews, T. K. Maycock, T. Waterfield, O. Yelekçi, R. Yu,
542 and B. Zhou, editors. *Climate Change 2021: The Physical Science Basis. Contribution of*
543 *Working Group I to the Sixth Assessment Report of the Intergovernmental Panel on*
544 *Climate Change*. Cambridge University Press.
- 545 Fick, S. E., and R. J. Hijmans. 2017. WorldClim 2: new 1-km spatial resolution climate surfaces
546 for global land areas. *International Journal of Climatology* 37:4302–4315.
- 547 Hamann, A., T. Wang, D. L. Spittlehouse, and T. Q. Murdock. 2013. A comprehensive, high-
548 resolution database of historical and projected climate surfaces for western North America.
549 *Bulletin of the American Meteorological Society* 94:1307–1309.
- 550 Hijmans, R. J., S. E. Cameron, J. L. Parra, P. G. Jones, and A. Jarvis. 2005. Very high resolution
551 interpolated climate surfaces for global land areas. *International Journal of Climatology*
552 25:1965–1978.

- 553 Hui, Y., Y. Xu, J. Chen, C. Y. Xu, and H. Chen. 2020. Impacts of bias nonstationarity of climate
554 model outputs on hydrological simulations. *Hydrology Research* 51:925–941.
- 555 Hunter, R. D., and R. K. Meentemeyer. 2005. Climatologically aided mapping of daily
556 precipitation and temperature. *Journal of Applied Meteorology* 44:1501–1510.
- 557 Iturbide, M., J. M. Gutiérrez, L. M. Alves, J. Bedia, R. Cerezo-Mota, E. Gimadevilla, A. S.
558 Cofiño, A. Di Luca, S. H. Faria, I. V. Gorodetskaya, M. Hauser, S. Herrera, K. Hennessy,
559 H. T. Hewitt, R. G. Jones, S. Krakovska, R. Manzanar, D. Martínez-Castro, G. T. Narisma,
560 I. S. Nurhati, I. Pinto, S. I. Seneviratne, B. van den Hurk, and C. S. Vera. 2020. An update
561 of IPCC climate reference regions for subcontinental analysis of climate model data:
562 definition and aggregated datasets. *Earth System Science Data* 12:2959–2970.
- 563 Kanehama, T., I. Sandu, A. Beljaars, A. van Niekerk, and F. Lott. 2019. Which Orographic
564 Scales Matter Most for Medium-Range Forecast Skill in the Northern Hemisphere Winter?
565 *Journal of Advances in Modeling Earth Systems* 11:3893–3910.
- 566 Kelley, M., G. A. Schmidt, L. S. Nazarenko, S. E. Bauer, R. Ruedy, G. L. Russell, A. S.
567 Ackerman, I. Aleinov, M. Bauer, R. Bleck, V. Canuto, G. Cesana, Y. Cheng, T. L. Clune,
568 B. I. Cook, C. A. Cruz, A. D. Del Genio, G. S. Elsaesser, G. Faluvegi, N. Y. Kiang, D. Kim,
569 A. A. Lacis, A. Leboissetier, A. N. LeGrande, K. K. Lo, J. Marshall, E. E. Matthews, S.
570 McDermid, K. Mezuman, R. L. Miller, L. T. Murray, V. Oinas, C. Orbe, C. P. García-
571 Pando, J. P. Perlwitz, M. J. Puma, D. Rind, A. Romanou, D. T. Shindell, S. Sun, N.
572 Tausnev, K. Tsigaridis, G. Tselioudis, E. Weng, J. Wu, and M. S. Yao. 2020. GISS-E2.1:
573 Configurations and Climatology. *Journal of Advances in Modeling Earth Systems*
574 12:e2019MS002025.
- 575 Knutti, R. 2010. The end of model democracy? *Climatic Change* 102:395–404.
- 576 Lanzante, J. R., K. W. Dixon, M. J. Nath, C. E. Whitlock, and D. Adams-Smith. 2018. Some
577 pitfalls in statistical downscaling of future climate. *Bulletin of the American Meteorological*
578 *Society* 99:791–803.
- 579 Leduc, M., R. Laprise, R. de Elia, and L. Separovic. 2016. Is Institutional Democracy a Good
580 Proxy for Model Independence? *Journal of Climate* 29:8301–8316.
- 581 Lee, J. Y., J. Marotzke, G. Bala, L. Cao, S. Corti, J. P. Dunne, F. Engelbrecht, E. Fischer, J. C.
582 Fyfe, C. Jones, A. Maycock, J. Mutemi, O. Ndiaye, S. Panickal, and T. Zhou. 2021. Future
583 Global Climate: Scenario-Based Projections and Near-Term Information. Pages 4-1-4–195
584 in V. Masson-Delmotte, P. Zhai, A. Pirani, S. L. Connors, C. Péan, S. Berger, N. Caud, Y.
585 Chen, L. Goldfarb, M. I. Gomis, M. Huang, K. Leitzell, E. Lonnoy, J. B. R. Matthews, T.
586 K. Maycock, T. Waterfield, O. Yelekçi, R. Yu, and B. Zhou, editors. *Climate Change 2021:*
587 *The Physical Science Basis. Contribution of Working Group I to the Sixth Assessment*
588 *Report of the Intergovernmental Panel on Climate Change.* Cambridge University Press.
- 589 Liang, Y., N. P. Gillett, and A. H. Monahan. 2020. Climate Model Projections of 21st Century
590 Global Warming Constrained Using the Observed Warming Trend. *Geophysical Research*
591 *Letters* 47:1–10.

- 592 Lindvall, J., and G. Svensson. 2015. The diurnal temperature range in the CMIP5 models.
593 *Climate Dynamics* 44:405–421.
- 594 Maraun, D. 2016. Bias Correcting Climate Change Simulations - a Critical Review. *Current*
595 *Climate Change Reports* 2:211–220.
- 596 McSweeney, C. F., R. G. Jones, R. W. Lee, and D. P. Rowell. 2014. Selecting CMIP5 GCMs for
597 downscaling over multiple regions. *Climate Dynamics* 44:3237–3260.
- 598 Meehl, G. A., C. A. Senior, V. Eyring, G. Flato, J. F. Lamarque, R. J. Stouffer, K. E. Taylor, and
599 M. Schlund. 2020. Context for interpreting equilibrium climate sensitivity and transient
600 climate response from the CMIP6 Earth system models. *Science Advances* 6:1–11.
- 601 Milinski, S., N. Maher, and D. Olonscheck. 2019. How large does a large ensemble need to be?
602 *Earth System Dynamics Discussions*:1–19.
- 603 Müller, W. A., J. H. Jungclaus, T. Mauritsen, J. Baehr, M. Bittner, R. Budich, F. Bunzel, M.
604 Esch, R. Ghosh, H. Haak, T. Ilyina, T. Kleine, L. Kornblueh, H. Li, K. Modali, D. Notz, H.
605 Pohlmann, E. Roeckner, I. Stemmler, F. Tian, and J. Marotzke. 2018. A Higher-resolution
606 Version of the Max Planck Institute Earth System Model (MPI-ESM1.2-HR). *Journal of*
607 *Advances in Modeling Earth Systems* 10:1383–1413.
- 608 O’Neill, B. C., C. Tebaldi, D. P. Van Vuuren, V. Eyring, P. Friedlingstein, G. Hurtt, R. Knutti,
609 E. Kriegler, J. F. Lamarque, J. Lowe, G. A. Meehl, R. Moss, K. Riahi, and B. M. Sanderson.
610 2016. The Scenario Model Intercomparison Project (ScenarioMIP) for CMIP6.
611 *Geoscientific Model Development* 9:3461–3482.
- 612 Palazzi, E., L. Mortarini, S. Terzago, and J. von Hardenberg. 2019. Elevation-dependent
613 warming in global climate model simulations at high spatial resolution. *Climate Dynamics*
614 52:2685–2702.
- 615 Pierce, D. W., T. P. Barnett, B. D. Santer, and P. J. Gleckler. 2009. Selecting global climate
616 models for regional climate change studies. *Proceedings of the National Academy of*
617 *Sciences of the United States of America* 106:8441–8446.
- 618 Ribes, A., S. Qasmi, and N. P. Gillett. 2021. Making climate projections conditional on historical
619 observations. *Science Advances* 7:1–10.
- 620 Rupp, D. E., J. T. Abatzoglou, K. C. Hegewisch, and P. W. Mote. 2013. Evaluation of CMIP5
621 20th century climate simulations for the Pacific Northwest USA. *Journal of Geophysical*
622 *Research Atmospheres* 118:10884–10906.
- 623 Salathé, E. P., R. Steed, C. F. Mass, and P. H. Zahn. 2008. A high-resolution climate model for
624 the U.S. Pacific northwest: Mesoscale feedbacks and local responses to climate change.
625 *Journal of Climate* 21:5708–5726.
- 626 Sférian, R., P. Nabat, M. Michou, D. Saint-Martin, A. Voldoire, J. Colin, B. Decharme, C.
627 Delire, S. Berthet, M. Chevallier, S. Sénési, L. Franchisteguy, J. Vial, M. Mallet, E.

- 628 Joetzjer, O. Geoffroy, J. F. Guérémy, M. P. Moine, R. Msadek, A. Ribes, M. Rocher, R.
629 Roehrig, D. Salas-y-Méla, E. Sanchez, L. Terray, S. Valcke, R. Waldman, O. Aumont, L.
630 Bopp, J. Deshayes, C. Éthé, and G. Madec. 2019. Evaluation of CNRM Earth System
631 Model, CNRM-ESM2-1: Role of Earth System Processes in Present-Day and Future
632 Climate. *Journal of Advances in Modeling Earth Systems* 11:4182–4227.
- 633 Sellar, A. A., C. G. Jones, J. P. Mulcahy, Y. Tang, A. Yool, A. Wiltshire, F. M. O’Connor, M.
634 Stringer, R. Hill, J. Palmieri, S. Woodward, L. de Mora, T. Kuhlbrodt, S. T. Rumbold, D. I.
635 Kelley, R. Ellis, C. E. Johnson, J. Walton, N. L. Abraham, M. B. Andrews, T. Andrews, A.
636 T. Archibald, S. Berthou, E. Burke, E. Blockley, K. Carslaw, M. Dalvi, J. Edwards, G. A.
637 Folberth, N. Gedney, P. T. Griffiths, A. B. Harper, M. A. Hendry, A. J. Hewitt, B. Johnson,
638 A. Jones, C. D. Jones, J. Keeble, S. Liddicoat, O. Morgenstern, R. J. Parker, V. Predoi, E.
639 Robertson, A. Siahann, R. S. Smith, R. Swaminathan, M. T. Woodhouse, G. Zeng, and M.
640 Zerroukat. 2019. UKESM1: Description and Evaluation of the U.K. Earth System Model.
641 *Journal of Advances in Modeling Earth Systems* 11:4513–4558.
- 642 Sherwood, S., M. J. Webb, J. D. Annan, K. C. Armour, P. M. Forster, J. C. Hargreaves, G.
643 Hegerl, S. A. Klein, K. D. Marvel, E. J. Rohling, M. Watanabe, T. Andrews, P. Braconnot,
644 C. S. Bretherton, G. L. Foster, Z. Hausfather, A. S. von der Heydt, R. Knutti, T. Mauritsen,
645 J. R. Norris, C. Proistosescu, M. Rugenstein, G. A. Schmidt, K. B. Tokarska, and M. D.
646 Zelinka. 2020. An assessment of Earth’s climate sensitivity using multiple lines of
647 evidence. *Reviews of Geophysics*:0–2.
- 648 Sutton, R. T. 2018. ESD Ideas: A simple proposal to improve the contribution of IPCC WGI to
649 the assessment and communication of climate change risks. *Earth System Dynamics*
650 9:1155–1158.
- 651 Sutton, R. T., and E. Hawkins. 2020. ESD Ideas : Global climate response scenarios for IPCC
652 assessments:751–754.
- 653 Swart, N. C., J. N. S. Cole, V. V. Kharin, M. Lazare, J. F. Scinocca, N. P. Gillett, J. Anstey, V.
654 Arora, J. R. Christian, S. Hanna, Y. Jiao, W. G. Lee, F. Majaess, O. A. Saenko, C. Seiler, C.
655 Seinen, A. Shao, M. Sigmond, L. Solheim, K. Von Salzen, D. Yang, and B. Winter. 2019.
656 The Canadian Earth System Model version 5 (CanESM5.0.3). *Geoscientific Model*
657 *Development* 12:4823–4873.
- 658 Tabor, K., and J. W. Williams. 2010. Globally downscaled climate projections for assessing the
659 conservation impacts of climate change. *Ecological Applications* 20:554–565.
- 660 Tatebe, H., T. Ogura, T. Nitta, Y. Komuro, K. Ogochi, T. Takemura, K. Sudo, M. Sekiguchi, M.
661 Abe, F. Saito, M. Chikira, S. Watanabe, M. Mori, N. Hirota, Y. Kawatani, T. Mochizuki, K.
662 Yoshimura, K. Takata, R. O’ishi, D. Yamazaki, T. Suzuki, M. Kurogi, T. Kataoka, M.
663 Watanabe, and M. Kimoto. 2018. Description and basic evaluation of simulated mean state,
664 internal variability, and climate sensitivity in MIROC6. *Geoscientific Model Development*
665 12:2727–2765.
- 666 Taylor, K. E., R. J. Stouffer, and G. A. Meehl. 2012. An overview of CMIP5 and the experiment
667 design. *Bulletin of the American Meteorological Society* 93:485–498.

- 668 Volodin, E. M., E. V. Mortikov, S. V. Kostykin, V. Y. Galin, V. N. Lykossov, A. S. Gritsun, N.
669 A. Diansky, A. V. Gusev, and N. G. Iakovlev. 2017. Simulation of the present-day climate
670 with the climate model INMCM5. *Climate Dynamics* 49:3715–3734.
- 671 Wang, K., and G. D. Clow. 2020. The diurnal temperature range in CMIP6 models: Climatology,
672 variability, and evolution. *Journal of Climate* 33:8261–8279.
- 673 Wang, T., A. Hamann, D. Spittlehouse, and C. Carroll. 2016. Locally downscaled and spatially
674 customizable climate data for historical and future periods for North America. *Plos One*
675 11:e0156720.
- 676 Wang, T., A. Hamann, D. L. Spittlehouse, and T. Q. Murdock. 2012. ClimateWNA: high-
677 resolution spatial climate data for western North America. *Journal of Applied Meteorology*
678 and *Climatology* 51:16–29.
- 679 Wilby, R. L., S. P. Charles, E. Zorita, B. Timbal, P. Whetton, and L. O. Mearns. 2004.
680 Guidelines for Use of Climate Scenarios Developed from Statistical Downscaling Methods.
681 Page IPCC Task Group on Data and Scenario Support for Impact and Climate Analysis
682 (TGICA).
- 683 Wilson, L. J., M. Vallee, and J. Montpetit. 2008. Comments on “Hydrometeorological Accuracy
684 Enhancement via Postprocessing of Numerical Weather Forecasts in Complex Terrain.”
685 *Weather and Forecasting* 24:892–894.
- 686 Wu, T., Y. Lu, Y. Fang, X. Xin, L. Li, W. Li, W. Jie, J. Zhang, Y. Liu, L. Zhang, F. Zhang, Y.
687 Zhang, F. Wu, J. Li, M. Chu, Z. Wang, X. Shi, X. Liu, M. Wei, A. Huang, Y. Zhang, and X.
688 Liu. 2019. The Beijing Climate Center Climate System Model (BCC-CSM): The main
689 progress from CMIP5 to CMIP6. *Geoscientific Model Development* 12:1573–1600.
- 690 Yukimoto, S., H. Kawai, T. Kosshiro, N. Oshima, K. Yoshida, S. Urakawa, H. Tsujino, M.
691 Deushi, T. Tanaka, M. Hosaka, S. Yabu, H. Yoshimura, E. Shindo, R. Mizuta, A. Obata, Y.
692 Adachi, and M. Ishii. 2019. The meteorological research institute Earth system model
693 version 2.0, MRI-ESM2.0: Description and basic evaluation of the physical component.
694 *Journal of the Meteorological Society of Japan* 97:931–965.
- 695 Ziehn, T., M. A. Chamberlain, R. M. Law, A. Lenton, R. W. Bodman, M. Dix, L. Stevens, Y. P.
696 Wang, and J. Srbinovsky. 2020. The Australian Earth System Model: ACCESS-ESM1.5.
697 *Journal of Southern Hemisphere Earth Systems Science* 70:193–214.
- 698